

# Modeling of two rings -photonic crystal fibers with the scalar – finite element method

L. CHERBI<sup>a</sup>, A. BELLALIA<sup>a</sup>, M. UTHMAN<sup>b</sup>, A. BISWAS<sup>c,d\*</sup>

<sup>a</sup>Laboratory of Instrumentation, U.S.T.H.B University, B.P 32 El Alia Bab-Ezzouar 16111 Algiers, Algeria

<sup>b</sup>School of Engineering and Mathematical Sciences, City University London, EC1V 0HB London, U.K

<sup>c</sup>Department of Mathematical Sciences Delaware, State University Dover, DE 19901-2277, USA

<sup>d</sup>Department of Mathematics, King Abdulaziz University, PO Box 80203, Jeddah-21589, Saudi Arabia

We arrived to conceive a numerical model based on the scalar finite element method to investigate numerically, in few seconds, the fundamental characteristics of propagation in two – ring photonic crystal fibers such as effective index of fundamental mode, its confinement and chromatic dispersion. Control and annulment of the chromatic dispersion for small wavelength have also been touched upon.

(Received March 18, 2013; accepted November 7, 2013)

**Keywords:** Photonic Crystal Fiber (PCF), Scalar Finite Element method (SC-FEM), Confinement loss, Chromatic dispersion

## 1. Introduction

The technological aspect of PCF is pretty varied and research in this area is quite vast [1-4]. The waveguide properties of photonic crystal fibers are not from spatially varying glass composition, as in conventional optical fiber, but from an arrangement of very tiny and closely spaced air holes which go through the whole length of fiber. In contrast with standard optical fibers, photonic crystal fibers can be made of a single material and have several geometric parameters which can be manipulated offering large flexibility of design. Even more, these fibers offer also the possibility of light guiding in a hollow core, thus opening new perspectives in fields such as nonlinear fiber optics [5-17], fiber lasers, supercontinuum generation, particle guidance, and fiber sensors. Therefore, there is a high interest in the scientific community in order to employ photonic crystal fibers in all kind of fields. Numerical simulations play an important role for the design and modeling of PCFs. So far, various modeling methods have been developed such as effective index approach [18] [19], multipole method (MM) [20] [21], beam propagation method (BPM) [22]–[23], finite-difference method (FDM) [24], finite difference time-domain method (FDTD) [25][26], boundary element method [27] and finite-element method (FEM) [28-30]. The choice of modeling tool can impact the computational time, required computational resources, and limitations of the method.

However, the vectorial finite element solutions have been known to include nonphysical solutions [31]. It will be difficult to distinguish between the spurious and the physical modes of the guides. Scalar finite element formulation for the analysis of isotropic waveguide with arbitrary cross section, is widely used in optical waveguides[32]. This approach has its main advantages: the smaller matrix dimensions, less computer time, no

spurious modes and capability of easily computing higher order modes.

In this paper, the approximate scalar -finite element method is extended to the two rings-PCF for the investigation of its propagation characteristics by calculating the effective index of fundamental mode, determining the distribution of electric field and studying its confinement based on several opto-geometric parameters of the fiber. The obtained numerical results show a good agreement with full-vector (V-FEM) ones reported in literature. Besides, in order to test the rapidity of used algorithm based on SC-FEM, we have estimated the calculation time for each simulation with SC-FEM and compare it to the ones of V-FEM. The results reveal the clear reduction in calculation time with SC-FEM. Afterwards, this method is applied for analyzing the dispersion properties of this PCF by manipulation of the size of air holes in the cladding or rather strategically structuring its respective positions. We could to eliminate the chromatic dispersion at 966 nm while in standard fibers it is difficult to eliminate the dispersion for wavelengths less than 1275 nm.

## 2. Analysis method

The SC-FEM is applied to solve the wave equation in a PCF. Its principle is based on weighted residuals method, especially Galerkin method. The SC-FEM approach is advantageous over the vectorial FEM (V-FEM) method. One of the main issues of the SC-FEM is that it has no spurious problem and the matrices in eigenvalues are small and symmetric and this results in the efficiency of the numerical algorithm and subsequently the computational time is far less than that of the V-FEM technique.

Galerkin's method consists in writing the unknown function as a linear combination of correctly weighted

functions that conform to the problem. This allows us to obtain a discrete or linear matrix system from basis functions. This choice allows accelerated numerical computation. In SC-FEM one starts from the Scalar wave equation:

$$\frac{\partial^2 \phi}{\partial x^2} + \frac{\partial^2 \phi}{\partial y^2} + k_0^2 (\epsilon_r - n_{eff}^2) \phi = 0 \quad (1)$$

Where  $\epsilon_r$  is the relative permittivity of the material,  $k_0$  is the wave number in the vacuum,  $n_{eff}$  is the effective index and  $\phi$  solves wave equation (1). Since this solution is unknown at this stage, it is necessary to find approximate solution  $\bar{\phi}$  that generates an error residual “R” in a right-hand of equation (1) which means:

$$\frac{\partial^2 \bar{\phi}}{\partial x^2} + \frac{\partial^2 \bar{\phi}}{\partial y^2} + k_0^2 (\epsilon_r - n_{eff}^2) \bar{\phi} = R \quad (2)$$

Then, the solution  $\bar{\phi}$  should be constructed so that the integral of the residual will be zero for some choices of weighted functions  $\psi$ . Therefore, this implies:

$$\iint \psi R \, dx \, dy = 0 \quad (3)$$

Substituting R from (2) into (3) and carrying out the integration by parts in (3), gives

$$\left[ \int \psi \frac{\partial \bar{\phi}}{\partial x} \, dy + \int \psi \frac{\partial \bar{\phi}}{\partial y} \, dx \right] - \iint \left( \frac{\partial \psi}{\partial x} \frac{\partial \bar{\phi}}{\partial x} + \frac{\partial \psi}{\partial y} \frac{\partial \bar{\phi}}{\partial y} \right) \, dx \, dy + \iint \psi k_0^2 (\epsilon_r - n_{eff}^2) \bar{\phi} \, dx \, dy = 0 \quad (4)$$

Then equation (4) can be rewritten as:

$$\left[ \int_{\Gamma} \psi \frac{\partial \bar{\phi}}{\partial n} \, d\Gamma \right] - \iint \left( \frac{\partial \psi}{\partial x} \frac{\partial \bar{\phi}}{\partial x} + \frac{\partial \psi}{\partial y} \frac{\partial \bar{\phi}}{\partial y} \right) \, dx \, dy + \iint \psi k_0^2 (\epsilon_r - n_{eff}^2) \bar{\phi} \, dx \, dy = 0 \quad (5)$$

Where  $\int_{\Gamma} d\Gamma$  represents the line integral calculus at the boundary  $\Gamma$  and  $\partial/\partial n$  is the derivative with respect to the normal vector n.

By applying the SC-FEM, the analysis region is divided into many triangular elements “e” of three nodes, an equation in one such element is given by:

$$\left[ \int_{\Gamma_e} \psi_e \frac{\partial \bar{\phi}_e}{\partial n} \, d\Gamma \right] - \iint_e \left( \frac{\partial \psi_e}{\partial x} \frac{\partial \bar{\phi}_e}{\partial x} + \frac{\partial \psi_e}{\partial y} \frac{\partial \bar{\phi}_e}{\partial y} \right) \, dx \, dy + \iint_e \psi_e k_0^2 (\epsilon_r - n_{eff}^2) \bar{\phi}_e \, dx \, dy = 0 \quad (6)$$

In the Galerkin method, both the approximate wave function  $\bar{\phi}_e$  and the weight function  $\psi_e$  are expanded by the same basis function  $N_e$  and thus we get:

$$\psi_e = \sum_i^3 \phi_{ei} N_i = [N_e]^T \{\phi_e\} \quad (7)$$

$$\bar{\phi}_e = \sum_i^3 \phi_{ei} N_i = [N_e]^T \{\phi_e\} \quad (8)$$

Where

$N_i$ : The basis functions

$\phi_{ei}$ : The field component at each node

By substituting (7) and (8) in equation (6), we find in each element e:

$$\{\phi_e\}^T \iint_e \left\{ \frac{\partial [N_e]}{\partial x} \frac{\partial [N_e]^T}{\partial x} + \frac{\partial [N_e]}{\partial y} \frac{\partial [N_e]^T}{\partial y} + k_0^2 (\epsilon_r - n_{eff}^2) [N_e] [N_e]^T \right\} \, dx \, dy \{\phi_e\} + \left[ \int_{\Gamma_e} \bar{\phi}_e \frac{\partial \phi_e}{\partial n} \, d\Gamma \right] = 0 \quad (9)$$

$$= \{\phi_e\}^T ([A_e] - \lambda^2 [B_e]) \{\phi_e\} - \left[ \int_{\Gamma_e} \bar{\phi}_e \frac{\partial \phi_e}{\partial n} \, d\Gamma \right] = 0 \quad (10)$$

Where

$$[A_e] = \iint_e \left( \frac{\partial [N_e]}{\partial x} \frac{\partial [N_e]^T}{\partial x} + \frac{\partial [N_e]}{\partial y} \frac{\partial [N_e]^T}{\partial y} \right) \, dx \, dy \quad (11)$$

$$[B_e] = \iint_e [N_e] [N_e]^T \, dx \, dy \quad (12)$$

$$\lambda^2 = k_0^2 (\epsilon_r - n_{eff}^2) \quad (13)$$

The next step of the SC-FEM is to assemble the contributions of all triangles of the region of interest to obtain:

$$\{\phi\}^T ([A] - \lambda^2 [B]) \{\phi\} - \sum_e \left[ \int_{\Gamma_e} \bar{\phi}_e \frac{\partial \phi_e}{\partial n} \, d\Gamma \right] = 0 \quad (14)$$

Where

$$\{\phi\} = \sum_e \{\phi_e\}, \quad [A] = \sum_e [A_e], \quad [B] = \sum_e [B_e] \quad (15)$$

Upon assuming that the wave function  $\phi_e$  and its normal derivative  $\frac{\partial \phi_e}{\partial n}$  are continuous, so the second term of equation (10) becomes:

$$-\left( \oint_{\Gamma} \bar{\phi} \frac{\partial \bar{\phi}}{\partial n} d\Gamma \right) \tag{16}$$

Substituting equation (16) in (14), we get:

$$\{\phi\}^T ([A] - \lambda^2 [B]) \{\phi\} - \left( \oint_{\Gamma} \bar{\phi} \frac{\partial \bar{\phi}}{\partial n} d\Gamma \right) = 0 \tag{17}$$

The second term of the equation (17) becomes zero by the Dirichlet condition and therefore equation (17) modifies to:

$$\{\phi\}^T ([A] - \lambda^2 [B]) \{\phi\} = 0 \tag{18}$$

We finally get an eigenvalue matrix equation that needs to be addressed as:

$$([A] - \lambda^2 [B]) \{\phi\} = 0 \tag{19}$$

The equation (19) can also be written in this form:

$$([K] - \beta^2 [M]) \{\phi\} = 0 \tag{20}$$

Where

$$[K] = \sum_e \left\{ \begin{aligned} & - \iint_e \left( \frac{\partial [N_e]}{\partial x} \frac{\partial [N_e]^T}{\partial x} + \frac{\partial [N_e]}{\partial y} \frac{\partial [N_e]^T}{\partial y} \right) dx dy \\ & + k_0^2 \epsilon_r \iint_e [N_e][N_e]^T dx dy \end{aligned} \right\} \tag{21}$$

$$= \sum_e \{ -([A_e] + [B_e]) + k_0^2 [C_e] \}$$

$$[M] = \sum_e \left\{ \iint_e [N_e][N_e]^T dx dy \right\} \tag{22}$$

$$= \sum_e [C_e]$$

$$\{\phi\} = \sum_e \{\phi_e\}$$

The square of the propagation constant  $\beta$  is an eigenvalue and  $\phi$  is an eigenvector.

The determination of matrix  $[k]$  in equation (21) needs to calculate  $[A_e]$ ,  $[B_e]$  and  $[C_e]$  as:

$$[A_e] = \iint_e \frac{\partial [N_e]}{\partial x} \frac{\partial [N_e]^T}{\partial x} dx dy \tag{23}$$

$$[B_e] = \iint_e \frac{\partial [N_e]}{\partial y} \frac{\partial [N_e]^T}{\partial y} dx dy \tag{24}$$

$$[C_e] = \iint_e [N_e][N_e]^T dx dy \tag{25}$$

The shape function  $[N_e]$  is expressed by area coordinates  $L_1, L_2, L_3$ , permitting to calculate integrals in Eqs (23) – (25). These coordinates are written as:

$$L_1 = \frac{Q_1(x - x_2) + R_1(y - y_2)}{2S_e},$$

$$L_2 = \frac{Q_2(x - x_3) + R_2(y - y_3)}{2S_e}$$

$$L_3 = \frac{Q_3(x - x_1) + R_3(y - y_1)}{2S_e}$$

Where  $Q_1 = y_2 - y_3, Q_2 = y_3 - y_1, Q_3 = y_1 - y_2, R_1 = x_2 - x_3, R_2 = x_3 - x_1, R_3 = x_1 - x_2$  and  $S_e = \frac{1}{2}[(y_3 - y_1)(x_2 - x_1) - (x_3 - x_1)(y_2 - y_1)]$  which is the area of the first order triangle,  $x_i$  and  $y_i$  ( $i=1:3$ ) are the coordinates of the three nodes of the triangle  $e$ .

Next, the matrices  $[A_e][B_e][C_e]$  of all element are combined to obtain the global matrices  $[K]$  and  $[M]$  after paying attention to the rows and columns. The obtained global matrix system will be solved to eventually obtain the propagation constant of guided modes and their eigen vectors.

### 3. Results

#### 3.1. SC- FEM Modal Solution for PCF

First, we demonstrate the application of the SC-FEM to study the properties of fundamental mode  $E_{11}^x$  in photonic crystal fibers. In this study, we consider index guiding silica PCF with two rings of 18 air holes arranged in a triangular lattice with the diameter of an air hole denoted by  $d$  and the distance (pitch) between two air holes by  $\Lambda$ .

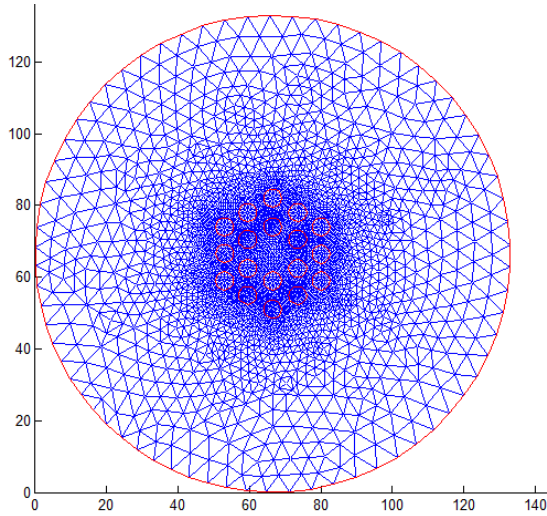


Fig. 1. The cross section of PCF with its triangulation (7808 triangles)

The refractive index of the silica used is taken as 1.4402 at an operating wavelength of 1.55  $\mu\text{m}$ . The SC-FEM model employs a typical division of the cross section of PCF into 7808 triangular elements of first order as it is shown in Fig. 1.

The Fig. 2 shows the variations of the effective indices of the fundamental mode  $E_{11}^x$  computed by the SC-FEM, with respect to the wavelengths for  $d/\Lambda=0.625$  and  $\Lambda=8\mu\text{m}$ . In the same figure we represented the values of effective indices of the same mode calculated with the variational FEM [32][33] where we see that the results are in good agreement especially for large wavelengths. This is also confirmed in the figure3 where we represented the variation of effective indices calculated with SC -FEM and variational FEM, respectively for  $d/\Lambda=0.5$  and  $\Lambda=8\mu\text{m}$ .

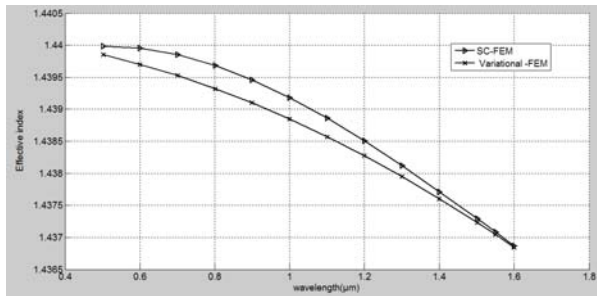


Fig. 2. Effective index of  $E_{11}^x$  over wavelength in a PCF of two rings of 18 circular holes and  $d/\Lambda=0.625$ .

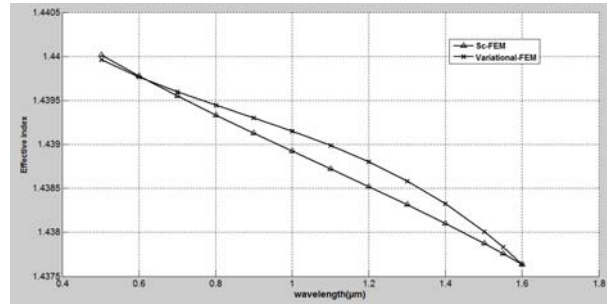


Fig. 3. Effective index of  $E_{11}^x$  over wavelength in a PCF of two rings of 18 circular holes and  $d/\Lambda=0.5$ .

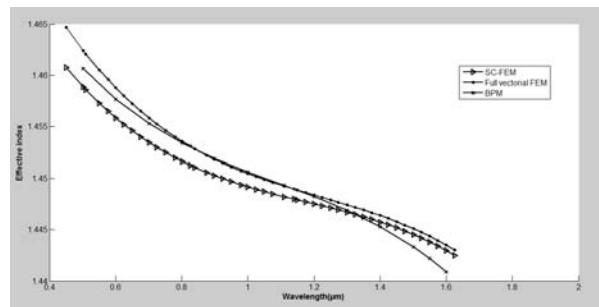


Fig. 4. Effective index of  $E_{11}^x$  over wavelength in a PCF of two rings of 18 circular holes and  $d/\Lambda=0.5$ , calculated with three numerical methods.

Next, we include the wavelength dependent refractive index of core during the finite element analysis of the SC-FEM using Sellmier expansion. Inclusion of wavelength dependent material dispersion in our model is more realistic. The interval of guidance  $[n_{\text{FSM}} \ n_{\text{core}}]$  will vary according to the wavelength in this case, where  $n_{\text{FSM}}$  is effective index of Fundamental Space filling Mode. In Fig. 4, we represent the variation of effective indices of  $E_{11}^x$  in a PCF of  $d/\Lambda=0.5$ , calculated with three different models: SC-FEM, Full vectorial FEM [34] and BPM. It can be seen that the obtained results are in a good agreement. We have also tested the computation time for the SC-FEM and Full Vectorial FEM, where it was noted that the time of computation in the SC-FEM doesn't exceed 20s while the full Vectorial FEM consumes a longer time (60-127s).

One clearly demonstrated in several researchs [35] that increasing the number of air-hole rings decreases the confinement loss exponentially while the design parameters of the photonic crystal fiber  $d$  and  $\Lambda$  have the most significant effect on dispersion.

In the next stage, the impact of varying the operating wavelength on the confinement of fundamental mode is studied for a PCF of two rings. Figures (5a) and (5 b) illustrate the mode confinement for two different wavelengths of 1000nm and 1400nm, respectively, for a value of  $d/\Lambda = 0.625$ ,  $D_{\text{core}}=11\mu\text{m}$ ,  $d =5 \mu\text{m}$  and  $\Lambda =8 \mu\text{m}$ .

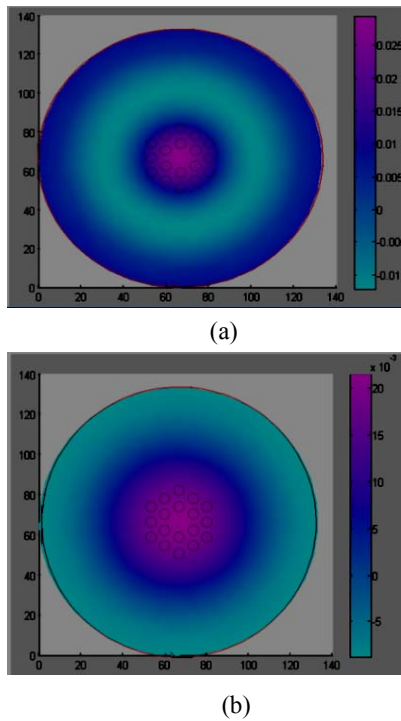


Fig. 5. Transverse repartition of fundamental mode  $E_{11}^x$  in PCF of two rings and for  $\Lambda=0.625$ , (a)  $\lambda=1000nm$ , (b)  $\lambda=1400nm$ .

Based on the (Fig. 5.a), one can conclude that when the fundamental mode is pretty well confined to the core with short wavelengths, its effective index is close to the refractive index of the core. On the other hand, when the mode is confined little for large wavelengths (figure 5.b) because an important part of the energy propagates through the cladding, the effective index of the fundamental mode decreases while getting closer to the index of the cladding, which agrees with earlier research result [35].

**3.2.Control of Dispersion**

The chromatic dispersion is subtracted from the variation of the effective index of fundamental mode, calculated by the SC-FEM method, according to the wavelength and by using the technique of Sellmeier of the silica according to wavelength. We varied the parameters of the PCF’s structure to see their impact on the variation of effective index versus the wavelength, the chromatic dispersion and its vanishing. We noted that adjustment of  $d$  and  $\Lambda$  could give very interesting results for the control of dispersion.

The Fig. 6.a depicts the variation of the effective index of the fundamental mode according to the wavelength in the PCF of  $d/\Lambda=0,5$ .

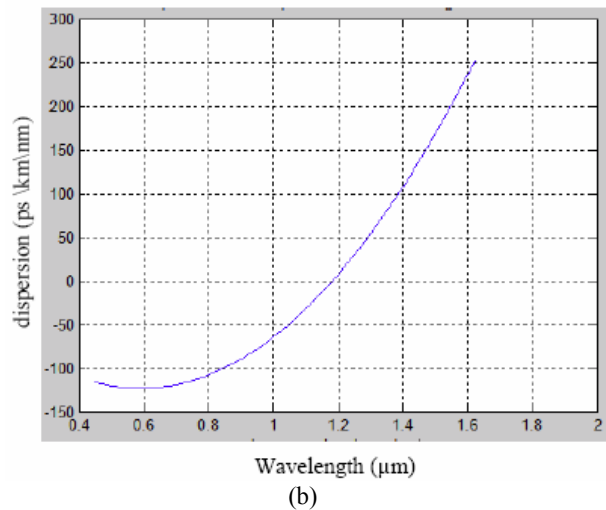
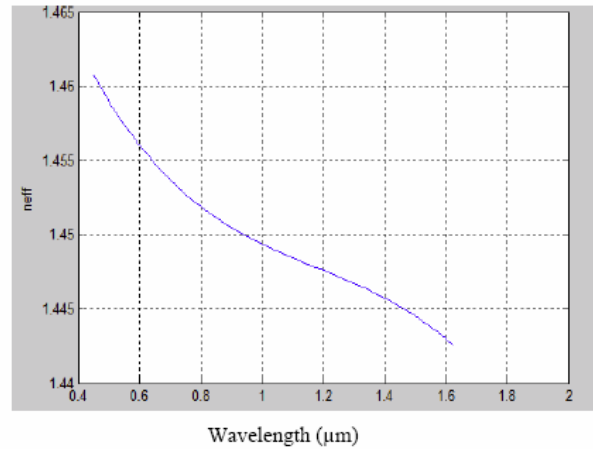
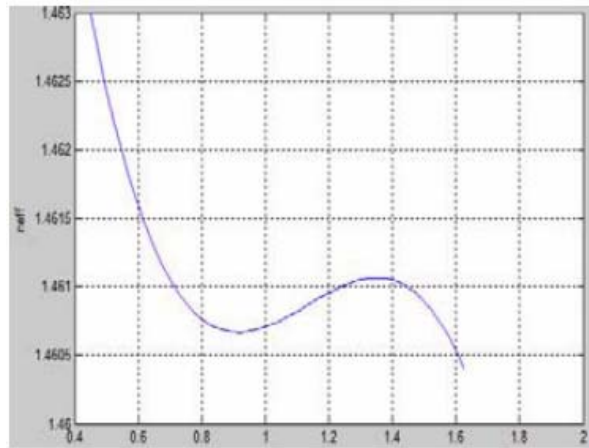


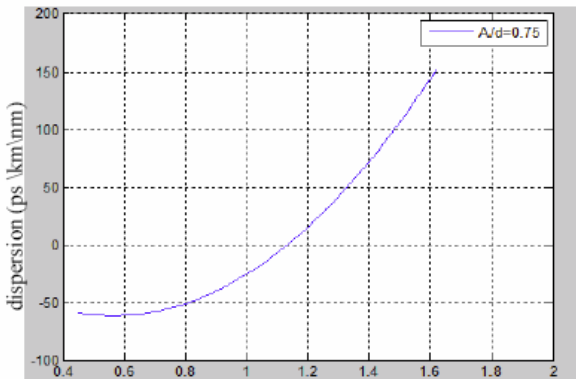
Fig. 6. Effective index of fundamental mode over wavelength for  $d/\Lambda=0.5$  (a) Chromatic dispersion versus wavelength (b).

From the simulations illustrated in the figure (6.a), we note that the effective index varies strongly: from 1.461016 to 1.442843. It is at the source of big diversity in the features of dispersion of the PCF according to their profile of index. We observe that the zero dispersion is close to 1186nm (Fig. 6.b).



Wavelength (μm)

(a)



Wavelength (μm)

(b)

Fig. 7. Effective index of fundamental mode over wavelength for  $d/\Lambda=0.75$  (a) Chromatic dispersion versus wavelength (b).

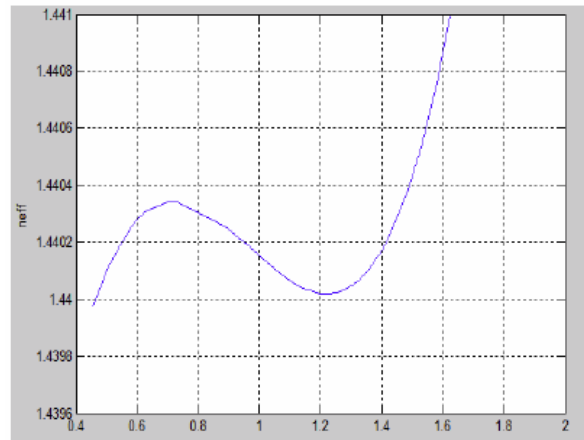
We also observe from the Fig. (7.a) that the effective index for this structure of PCF, increases and decreases with the wavelength and does not vary with a large step. As shows the figure 7.b, the zero of chromatic dispersion of PCF with  $d/\Lambda=0,75$  is about 1125nm.

Subsequently, we wanted to shift the zero of dispersion to lower wavelengths close to 1000nm by varying the diameter of the air holes and the pitch  $\Lambda$ .

In the figure (8.a), one represent the variation of effective index according to wavelength by choosing ( $d/\Lambda = 0,625$ ). One can conclude that the effective index increases and decreases with the wavelength when the ratio  $d/\Lambda$  increases, thing that one can exploit in the annulment of the chromatic dispersion.

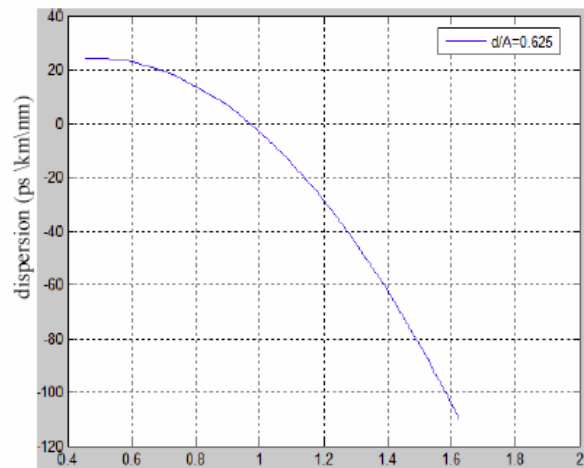
According to the plot in Fig. (8.b), we got the zero dispersion in the neighborhood of 966 nm in a PCF fiber with the geometric features (pitch =  $8\mu\text{m}$  and  $d=5\mu\text{m}$ ),

thing that doesn't happen in the standards fibers where the zero of dispersion cannot be smaller than 1275nm, it is due to the number of degrees of freedom that offers this PCF to nullify the chromatic dispersion when compared to standards fibers.



Wavelength (μm)

(a)



Wavelength (μm)

(b)

Fig. 8. Effective index of fundamental mode over wavelength for  $d/\Lambda=0.625$  (a) Chromatic dispersion versus wavelength (b).

#### 4. Conclusion

We demonstrated in this work that the SC-FEM can be applied on the PCF to investigate numerically the features of propagation by determining the modal field distribution and calculating its effective index in very little time. Comparing the results with those of earlier studies it is evidenced that the efficiency of the SC-FEM method in

the modeling of the propagation in PCF fiber despite the simplification of the used mathematical algorithm.

We noted through the reported results about the features of fundamental mode in the two rings- PCF that are especially attractive for numerous applications as intensity sensors.

We also studied the vanishing of the chromatic dispersion in this fiber for short wavelengths. The different simulations that were done on this topic, allowed us to see the possibility of controlling the chromatic dispersion while adjusting the geometry of the PCF and this allowed us to nullify the chromatic dispersion about a wavelength of around of 966nm.

## References

- [1] S.E. Barkou, J. Broeng, A. Bjarklev, *Optics letters* **24**, 46 (1999).
- [2] E. Yablonovitch, T. J. Gmitter, K. M. Leung, *Physical Review Letters*. **67**, 2295 (1991)
- [3] Laurent Labonté, *Analyse théorique et expérimentale des principales caractéristiques du mode fondamental dans les fibres optiques microstructurées air/silice*, Thèse de doctorat Université de Limoges( 2005).
- [4] D. G. Ouzoumov, F. R. Ahmad, D. Muller, N. Vankataraman, M.T. Gallagher, M.G. Thomas, J. Silcox, K.W. Koch, A. L. Gaeta, *Science* **301**, 1702 ( 2003).
- [5] H. Leblond, D. Mihalache, *Physics Reports* **523**, 61 (2013).
- [6] Y. J. He, D. Mihalache, B. B. Hu, *J. Opt. Soc. Am. B* **27**, 2174 (2010).
- [7] H. Leblond, D. Kremer, D. Mihalache, *Phys. Rev. A* **81**, 033824 (2010)
- [8] D. Mihalache, D. Mazilu, F. Lederer, *Cent. Eur. J. Phys.* **8**, 77 (2010).
- [9] D. Mihalache, *Rom. Rep. Phys.* **62**, 697 (2010)
- [10] D. Mihalache, *Rom. Rep. Phys.* **62**, 99 (2010).
- [11] F. W. Ye, L. W. Dong, B. A. Malomed, D. Mihalache, B. B. Hu, *J. Opt. Soc. Am. B* **27**, 757 (2010).
- [12] H. Leblond, D. Mihalache, *J. Phys. A-Math. Theor.* **43**, 375205 (2010).
- [13] D. Mihalache, *J. Optoelectron. Adv. Mater.* **12**, 12 (2010).
- [14] D. Mihalache, *J. Optoelectron. Adv. Mater.* **13**, 1055 (2011).
- [15] H. Leblond, D. Mihalache, *J. Optoelectron. Adv. Mater.* **12**, 1 (2010).
- [16] S. Crutcher, A. Osei, Ahmet Yildirim, Anjan Biswas, *J. Optoelectron. Adv. Mater.* **14**, 29 (2012).
- [17] Anjan Biswas, Kaisar R. Khan, Atiqur Rahman, Ahmet Yildirim, T. Hayat, Omar M. Aldossary, *J. Optoelectron. Adv. Mater.* **14**, 571 (2012).
- [18] T. A. Birks, J. C. Knight, P. St. J. Russell, *Opt. Lett.* **22**, 961 (1997).
- [19] J. C. Knight, T. A. Birks, P. S. J. Russell, J. P. de Sandro, *J. Opt. Soc. Amer. A* **15**, 748 (1998).
- [20] M. J. Steel, T. P. White, C. M. de Sterke, R. C. McPhedran, L. C. Botten, *Opt. Lett.* **26**, 488 (2001).
- [21] B. T. Kuhlmeiy, T. P. White, G. Renversez, D. Maystre, L. C. Botten, C. M. de Sterke, R. C. McPhedran, *J. Opt. Soc. Amer. B* **19**, 2331 (2002).
- [22] C. E. Kerbage, B. J. Eggleton, P. S. Westbrook, R. S. Windeler, *Experimental Opt. Express* **7**, 113 (2000).
- [23] F. Fogli, L. Saccomandi, P. Bassi, *Opt. Express* **10**, 54 (2002).
- [24] Z. Zhu, T. G. Brown, *Opt. Express* **10**, 853 (2002).
- [25] G. E. Town, J. T. Lizer, *Opt. Lett.* **26**, 1042 ( 2001).
- [26] M. Qiu, *Microw. Opt. Technol. Lett.* **30**, 327 (2001).
- [27] N. Guan, S. Habu, K. Takenaga, K. Himeno, A. Wada, *J. Lightw. Technol.* **21**, 1787 (2003).
- [28] A. Polycarpou, *Introduction to the Finite Element Method in Electromagnetics*, Morgan and Claypool (2006).
- [29] F. Brechet, J. Marcou, D. Pagnoux, P. Roy, *Opt. Fiber Technol.* **6**, 181 (2000).
- [30] S. Guenneau, A. Nicholet, F. Zolla, S. Lasquelllec, *IEEE Trans. Magn.* **38**, 1261 ( 2002).
- [31] B. M. Azizur Rahman, J. Brian Davies, *IEEE Trans. microw Theory & Techni*, **MTT-32**, 922 (1984).
- [32] Kenji Kawano, *introduction to optical waveguide Analysis*, Jhon Wiley (2001).
- [33] M. Azizur Rahman, Muhammad Uthman, Arti Agrawal, and Kenneth T. V. Grattan, *Applied Optics* **50**, 6505 (2011).
- [34] Uranus, Henri Hoekstra, H, *Optics Express* **12**, 2795 (2004).
- [35] Limin Xiao, Wei Jin, M.S. Demokan, *Optics Express* **15**, 15637 ( 2007).

\*Corresponding author: biswas.anjan@gmail.com